De novo carcinogenesis promoted by chronic inflammation is B lymphocyte dependent

Karin E. de Visser,[1] Lidiya V. Korets,[1] and Lisa M. Coussens[1,2,3,*]

[1]Cancer Research Institute, University of California, San Francisco, 2340 Sutter Street, San Francisco, California 94143
[2]Department of Pathology, University of California, San Francisco, 2340 Sutter Street, San Francisco, California 94143
[3]Comprehensive Cancer Center, University of California, San Francisco, 2340 Sutter Street, San Francisco, California 94143
*Correspondence: coussens@cc.ucsf.edu

Summary

Chronic inflammation predisposes tissue to cancer development; however, regulatory mechanisms underlying recruitment of innate leukocytes toward developing neoplasms are obscure. We report that genetic elimination of mature T and B lymphocytes in a transgenic mouse model of inflammation-associated de novo epithelial carcinogenesis, e.g., *K14-HPV16* mice, limits neoplastic progression to development of epithelial hyperplasias that fail to recruit innate immune cells. Adoptive transfer of B lymphocytes or serum from *HPV16* mice into T and B cell-deficient/*HPV16* mice restores innate immune cell infiltration into premalignant tissue and reinstates necessary parameters for full malignancy, e.g., chronic inflammation, angiogenic vasculature, hyperproliferative epidermis. These findings support a model in which B lymphocytes are required for establishing chronic inflammatory states that promote de novo carcinogenesis.

Introduction

Reciprocal interactions between genetically altered "initiated" cells, responding host cells such as fibroblasts, innate immune cells and vascular cells, and molecules undergoing remodeling in the surrounding microenvironment regulate efficient tumor development (Bissell and Radisky, 2001). The significance of innate immune cell involvement in cancer development has recently been recognized (Balkwill et al., 2005; Coussens and Werb, 2002). Initial circumstantial evidence linking inflammation with cancer was provided by clinical data correlating infiltration of innate immune cells into malignant tissue with poor clinical outcome (Coussens and Werb, 2002) and population-based studies revealing increased cancer incidence in individuals affected by chronic inflammatory disorders such as pancreatitis, Crohn's disease, and ulcerative colitis (Shacter and Weitzman, 2002; Thun et al., 2004). Causal demonstration of a functional link between inflammation and cancer has been provided by clinical studies reporting reduced cancer incidence in patients treated long-term with anti-inflammatory drugs (Turini and DuBois, 2002). Mechanistic in vivo studies have implicated proteolytic enzymes released by inflammatory cells (Coussens et al., 1999), transcription factor NFκB, and the potent proinflammatory cytokine tumor necrosis factor-α (Greten et al., 2004; Pikarsky et al., 2004) as functionally important proteins potentiating inflammation-associated cancer development. Taken together, there is compelling evidence indicating that identification of critical molecules involved in activating or sustaining chronic inflammation, or downstream molecules responding to activated innate immune cells, may provide efficacious cancer chemopreventative targets.

In mammals, organs are equipped with defense programs that facilitate rapid responses to tissue damage, e.g., activation of the complement system, mobilization of resident sentinel cells (dendritic cells, mast cells, macrophages), and increased levels of soluble proinflammatory mediators (Kupper and Fuhlbrigge, 2004). Acute mobilization of these pathways arrests tissue damage and removes "damaged" cells to restore tissue homeostasis. When critical parameters of these programs are dysregulated, chronic disease states result, e.g., lupus, Alzheimer's and heart disease, arthritis, asthma, pancreatitis, and inflammatory bowel disease (Firestein, 2003; Kupper and Fuhlbrigge, 2004). Mechanistic analysis of experimental animal models representative of some of these chronic disorders has revealed interactions between innate and adaptive immune cells as key determinants of disease pathogenesis (Gould et al., 2003; Ji et al., 2002). Since chronic inflammation is considered a risk factor for development of certain cancers (Thun et al., 2004), we hypothesized that similar interactions between innate and adaptive immune cells may potentiate malignant

SIGNIFICANCE

Despite compelling data indicating a functional link between inflammation and cancer, pathways regulating initiation of chronic inflammation during tumorigenesis are obscure. We demonstrate that B lymphocytes are critical for initiating chronic inflammation during premalignancy and thus support the concept that oncogene expression in "initiated" cells alone is not sufficient for full malignant progression. Instead, additional signals provided by adaptive and innate immune cells are required for elaboration of the malignant state. Our results suggest that pharmacological interventions targeting B lymphocytes and/or recruitment of innate immune cells toward premalignant tissue represent viable cancer chemopreventative strategies.

progression in at-risk "initiated" tissue. To address this, we took a genetic approach and utilized a transgenic mouse model of multistage epithelial carcinogenesis where early region genes of human papillomavirus type 16 (*HPV16*) are expressed as transgenes under control of the human keratin 14 (K14) promotor/enhancer, i.e., *K14-HPV16* mice (Arbeit et al., 1994), and intercrossed them with *R*ecombination-*A*ctivating *Gene*-1 homozygous null (*RAG-1*$^{-/-}$) mice deficient for mature B and T lymphocytes (Mombaerts et al., 1992). The consequence of adaptive immune deficiency in *HPV16* mice is failure to induce leukocyte recruitment and absence of chronic inflammation in premalignant skin. As a result, tissue levels of vascular endothelial growth factor-A (VEGF-A) and gelatinolytic metalloproteinases remain at steady-state levels, blood vasculature remains quiescent, oncogene-positive keratinocytes fail to attain a hyperproliferative phenotype, and carcinoma incidence is reduced. We report that transfer of B cells or serum from *HPV16* mice into *HPV16/RAG-1*$^{-/-}$ mice restores characteristic chronic inflammation in premalignant skin and reinstates regulatory mechanisms necessary for activation of angiogenic vasculature and keratinocyte hyperproliferation. Taken together, these data indicate that B cells play a crucial role in the onset of chronic inflammation associated with epithelial cancer development.

Results

Reduced infiltration of innate immune cells in premalignant skin of *HPV16/RAG-1*$^{-/-}$ mice

As is observed in human neoplasms (Takanami et al., 2000; Toth-Jakatics et al., 2000), premalignant skin in *HPV16* mice is characterized by infiltration of innate immune cells (Coussens et al., 1999; de Visser et al., 2004). Given the crucial role of the adaptive immune system during initiation of several inflammatory diseases (Gould et al., 2003; Lee et al., 2002), we hypothesized that B and/or T lymphocytes might contribute to activation of innate immune responses during early neoplastic progression in *HPV16* mice. To assess this, we generated *HPV16/RAG-1*$^{-/-}$, *HPV16/CD4*$^{-/-}$, *HPV16/CD8*$^{-/-}$, and *HPV16/CD4*$^{-/-}$*/CD8*$^{-/-}$ mice and examined key characteristics of premalignant progression in the presence or absence of complete or partial adaptive immunity.

Quantitative detection of CD45^{+} cells by flow cytometry revealed reduced infiltrates in premalignant skin of *HPV16/RAG-1*$^{-/-}$ mice as compared to *HPV16*, *HPV16/CD4*$^{-/-}$, *HPV16/CD8*$^{-/-}$, and *HPV16/CD4*$^{-/-}$*/CD8*$^{-/-}$ mice (Figure 1A). To investigate the nature of this reduced inflammatory infiltrate, we profiled two major leukocyte populations characteristic of *HPV16* premalignant skin, i.e., mast cells (MCs) and granulocytes, and found that both were significantly reduced in *HPV16/RAG-1*$^{-/-}$ as compared to age-matched *HPV16*, *HPV16/CD4*$^{-/-}$, *HPV16/CD8*$^{-/-}$, and *HPV16/CD4*$^{-/-}$*/CD8*$^{-/-}$ skin (Figures 1B and 1C). Thus, in the absence of B and T cells, chronic inflammation characteristic of premalignancy was significantly reduced.

Inflammation regulates characteristics of premalignancy

Chronic inflammation potentiates epithelial hyperproliferation, tissue remodeling, and development of angiogenic vasculature during premalignancy in *HPV16* mice (Coussens et al., 1999; van Kempen et al., 2002). These effects are, in part, mediated via release of bioactive mediators, growth factors, and extracellular proteases from leukocytes (Coussens et al., 1999; Coussens et al., 2000). Since leukocyte infiltration is significantly reduced in *HPV16/RAG-1*$^{-/-}$ skin (Figure 1), we hypothesized that characteristic parameters of premalignancy regulated by leukocytes (i.e., tissue remodeling, gelatinolytic activity, VEGF-A levels, development of angiogenic vasculature, and epithelial hyperproliferation) might also be attenuated.

We assessed gelatinolytic activity in lysates from premalignant skin of *HPV16* and *HPV16/RAG-1*$^{-/-}$ mice by enzyme solution assays (Rhee et al., 2004). Gelatinolytic activity in *HPV16* skin incrementally increased during premalignancy; however, no significant changes were observed in *HPV16/RAG-1*$^{-/-}$ skin (Figure 2A, left panel). We and others have previously reported that two gelatinolytic proteases from the matrix metalloproteinase (MMP) family, namely MMP-2 and MMP-9, functionally contribute to cancer development (Coussens et al., 2000; Giraudo et al., 2004); (Bergers et al., 2000); thus, we utilized gelatin substrate zymography to assess the presence of distinct molecular weight forms of MMP-2 and -9 in *HPV16/RAG-1*$^{-/-}$ lysates where we found only their latent forms, as compared to progressively increased amounts of both pro- and active forms in *HPV16* skin (Figure 2A, right panel).

MMP-9 is an important leukocyte-derived extracellular protease that functionally contributes to cancer development by potentiating epithelial hyperproliferation and activation of angiogenesis, in part by its ability to induce tissue remodeling and regulate bioavailability of extracellular matrix (ECM)-sequestered VEGF (Bergers et al., 2000; Bergers and Coussens, 2000). Thus, we reasoned that if leukocyte infiltration and levels of MMP-9 and other gelatinases were reduced in *HPV16/RAG-1*$^{-/-}$ skin, levels of VEGF-A might also be reduced, resulting in diminished development of angiogenic vasculature. We examined VEGF-A protein levels in skin lysates of *HPV16* mice by ELISA and found a progressive increase at each neoplastic stage (Figure 2B, upper left panel) that correlated with increasing percentages of CD31^{+} cells (Figure 2B, upper right panel) and development of angiogenic vasculature (Figure 2B, bottom panels). In contrast, age-matched skin from *HPV16/RAG-1*$^{-/-}$ mice failed to accumulate VEGF (Figure 2B) or demonstrate any characteristics of vascular activation associated with angiogenesis (i.e., increased percentage of CD31^{+} cells, vasodilation or vascular tortuosity; Figures 2B). Similarly, epithelial proliferation was markedly reduced in *HPV16/RAG-1*$^{-/-}$ versus age-matched *HPV16* skin (Figure 2C, left panel). Taken together, these data suggest that failure to efficiently recruit innate immune cells into premalignant skin results in reduced levels of tissue remodeling enzymes and VEGF, deficient development of angiogenic vasculature, and attenuated ability of keratinocytes to achieve hyperproliferative growth characteristics.

Decreased incidence of squamous cell carcinomas in *HPV16/RAG-1*$^{-/-}$ mice

To assess whether absent characteristics of premalignancy in *HPV16/RAG-1*$^{-/-}$ mice correlated with reduced carcinoma incidence, we monitored a cohort of *HPV16/RAG-1*$^{-/-}$ mice (n = 108) for cancer development as compared to a similar cohort of *HPV16* mice (n = 134). *HPV16/RAG-1*$^{-/-}$ mice developed hyperplastic skin lesions with a similar 100% penetrance as *HPV16* controls (Figure 2C). At 4 months of age, whereas

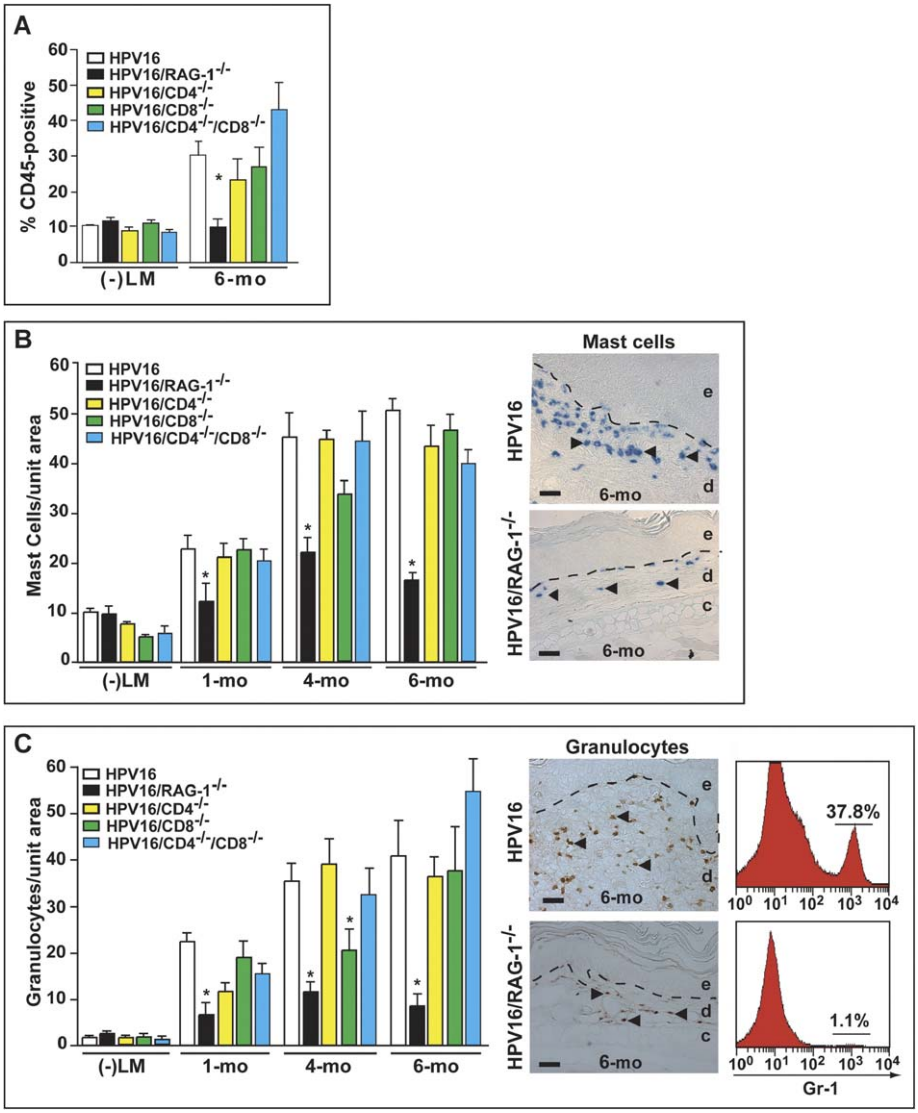

Figure 1. Reduced infiltration of innate immune cells in premalignant skin of *HPV16/RAG-1*$^{-/-}$ mice

A: Percentage of CD45^{+} cells in skin of negative littermates (−)LM and premalignant *HPV16*, *HPV16/RAG-1*$^{-/-}$, *HPV16/CD4*$^{-/-}$, *HPV16/CD8*$^{-/-}$, and *HPV16/CD4*$^{-/-}$*/CD8*$^{-/-}$ mice at 6 months of age analyzed by flow cytometry. Results shown are mean percentages (n = 3–7 mice). Error bars represent SEM and asterisks (*) indicate statistically significant differences between age-matched *HPV16* versus *HPV16/RAG-1*$^{-/-}$ mice ($p = 0.02$, Mann-Whitney).

B: Mast cells (arrowheads, blue staining) during premalignant progression in skin of (−)LM and transgenic mice. Values reflect averages from five high-power fields per mouse and five mice per category. Error bars represent SEM, asterisk (*) indicates statistically significant differences between age-matched *HPV16* versus *HPV16/RAG-1*$^{-/-}$ mice ($p < 0.05$, Mann-Whitney). Dashed line, epidermal-dermal interface; epidermis, e; dermis, d; cartilage, c. Scale bar, 50 μm.

C: Granulocytes during premalignant progression in skin of (−)LM and transgenic mice. Quantitative values (left panel) represent number of granulocytes (middle panel; arrowheads, brown stained cells), averaged from five high-power fields per mouse and five mice per category. Error bars represent SEM, and asterisk (*) indicates statistically significant differences between age-matched *HPV16* versus *HPV16/RAG-1*$^{-/-}$ or *HPV16/CD8*$^{-/-}$ mice ($p < 0.05$ Mann-Whitney). Histograms representing single-cell suspensions of premalignant *HPV16* and *HPV16/RAG-1*$^{-/-}$ skin (4 months of age) analyzed by flow cytometry. Scale bar, 50 μm.

100% of *HPV16* mice manifest focally dysplastic epidermis, this was not found in age-matched *HPV16/RAG-1*$^{-/-}$ mice; in fact, a mere 12% of *HPV16/RAG-1*$^{-/-}$ mice ever developed focally dysplastic epidermis (Figure 2C). Moreover, absence of B and T cells significantly reduced the overall incidence of invasive carcinomas in *HPV16/RAG-1*$^{-/-}$ mice, where only 6.4% of mice developed SCCs as compared to the ~47% in control *HPV16* mice ($p \leq 0.0045$, Log rank analysis; Figure 2C). This dramatic reduction in carcinoma incidence in *HPV16/RAG-1*$^{-/-}$ mice is in contrast to the modest reduction in *HPV16/CD4*$^{-/-}$ mice (41%) and characteristic ~50% incidence in *HPV16/CD8*$^{-/-}$ mice (Daniel et al., 2003).

Immunoglobulin deposition characterizes *HPV16* premalignant skin

Since genetic elimination of CD4^{+} and/or CD8^{+} cells did not alter leukocyte recruitment into premalignant *HPV16* as compared to *HPV16/RAG-1*$^{-/-}$ skin (Figure 1), we hypothesized that B cells might regulate innate immune cell response; however, B cells do not infiltrate premalignant *HPV16* skin (Figure 3A). B cells can however exert distal effects via production of immunoglobulins (Ig) that subsequently circulate in blood and accumulate in tissues where they regulate cellular pathways via engagement of complement proteins, formation of immune complexes, or activation of cell surface receptors on resident leukocytes (Firestein, 2003; Hogarth, 2002). Thus, we assessed spatial and temporal depositions of IgG, IgG1, IgG2a, IgM, IgA, and IgE in *HPV16* skin (Figure 3B). In nontransgenic skin, IgM and IgG immunoreactivity was detected in the dermis at low levels (Figure 3B), whereas IgG1, IgG2a, IgA, and IgE were not detected (data not shown). In contrast, moderate IgM and strong IgG immunoreactivity was detected in dermal stroma by 1 month of age in *HPV16* skin that became more pronounced by 6 month (Figure 3B). IgM was localized proximal to epithelial basement membranes, whereas extensive regions of IgG immunoreactivity were also detected throughout the dermis, reflecting IgG1 predominantly, and to a lesser extent IgG2a (Figure 3B). IgA and IgE immunoreactivity were not detected in

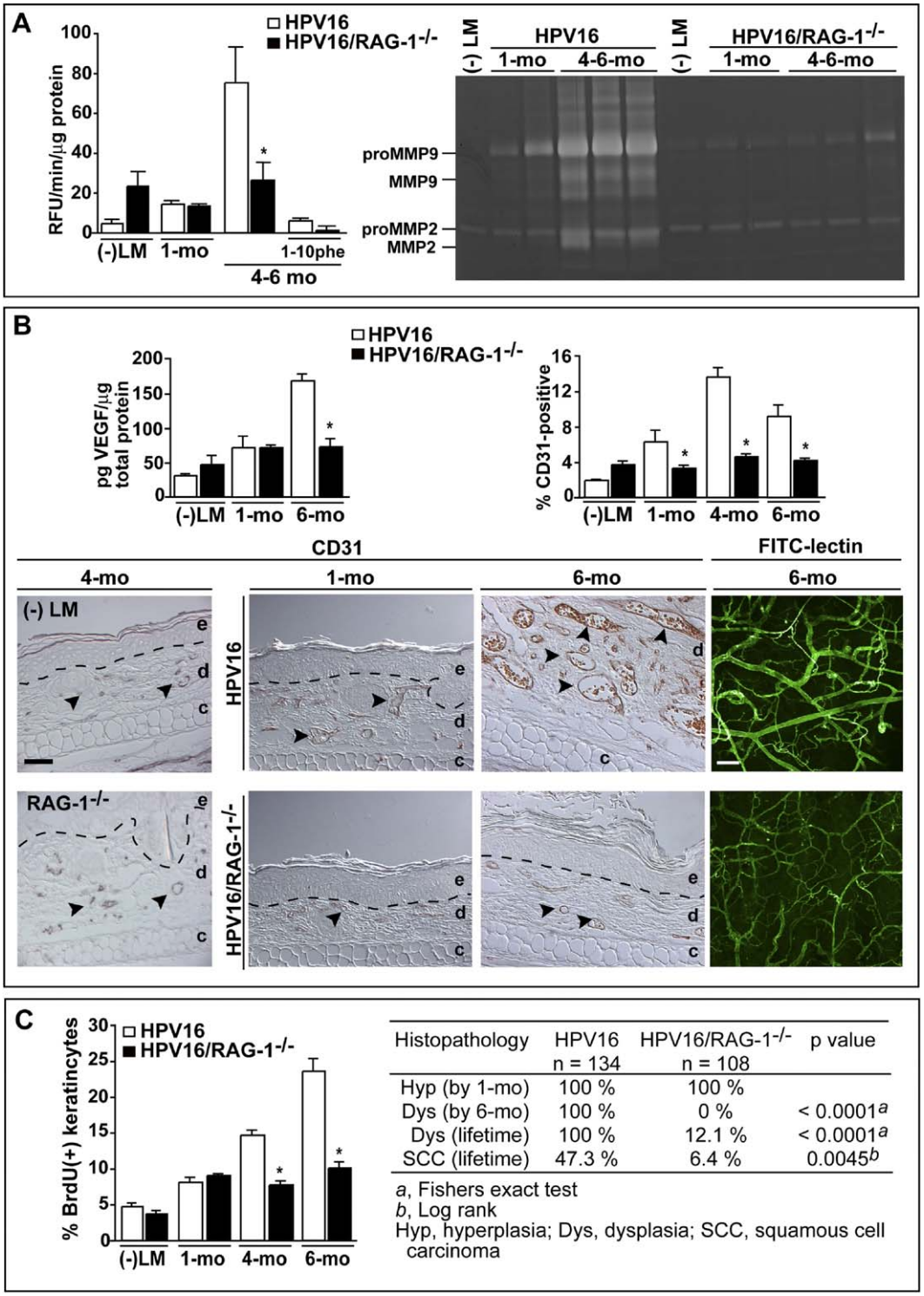

Histopathology	HPV16 n = 134	HPV16/RAG-1$^{-/-}$ n = 108	p value
Hyp (by 1-mo)	100 %	100 %	
Dys (by 6-mo)	100 %	0 %	< 0.0001[a]
Dys (lifetime)	100 %	12.1 %	< 0.0001[a]
SCC (lifetime)	47.3 %	6.4 %	0.0045[b]

a, Fishers exact test
b, Log rank
Hyp, hyperplasia; Dys, dysplasia; SCC, squamous cell carcinoma

Figure 2. Inflammation regulates neoplastic progression in *HPV16* mice

A: Gelatinolytic activities in tissue extracts from (−)LM, *HPV16*, and *HPV16/RAG-1*$^{-/-}$ mice measured by enzyme solution assay. Values represent average change in relative fluorescence units (RFU)/min/μg tissue protein (n = 3–5 per time point). Error bars represent SEM, and asterisk (*) indicates statistically significant differences between age-matched *HPV16* versus *HPV16/RAG-1*$^{-/-}$ mice ($p < 0.05$, Mann-Whitney). Tissue lysates from (−)LM, *HPV16*, and *HPV16/RAG-1*$^{-/-}$ mice were assessed for relative differences in levels of pro and/or active molecular weight forms of MMP-2 and -9 by gelatin substrate zymography.

B: VEGF-A protein levels in skin extracts from (−)LM, *HPV16*, and *HPV16/RAG-1*$^{-/-}$ mice assessed by ELISA. Percentage of CD31^{+} cells analyzed by flow cytometry in ears of (−)LM, *HPV16*, and *HPV16/RAG-1*$^{-/-}$ mice. Error bars represent SEM, and asterisk (*) indicates statistically significant differences between age-matched *HPV16* versus *HPV16/RAG-1*$^{-/-}$ mice ($p < 0.05$, unpaired t test). Immunolocalization of CD31 (arrowheads, brown staining) in age-matched skin from (−)LM, *HPV16*, and *HPV16/RAG-1*$^{-/-}$ mice. Dashed line, epidermal-dermal interface; epidermal, e; dermal, d; cartilage, c. Scale bar, 50 μm.

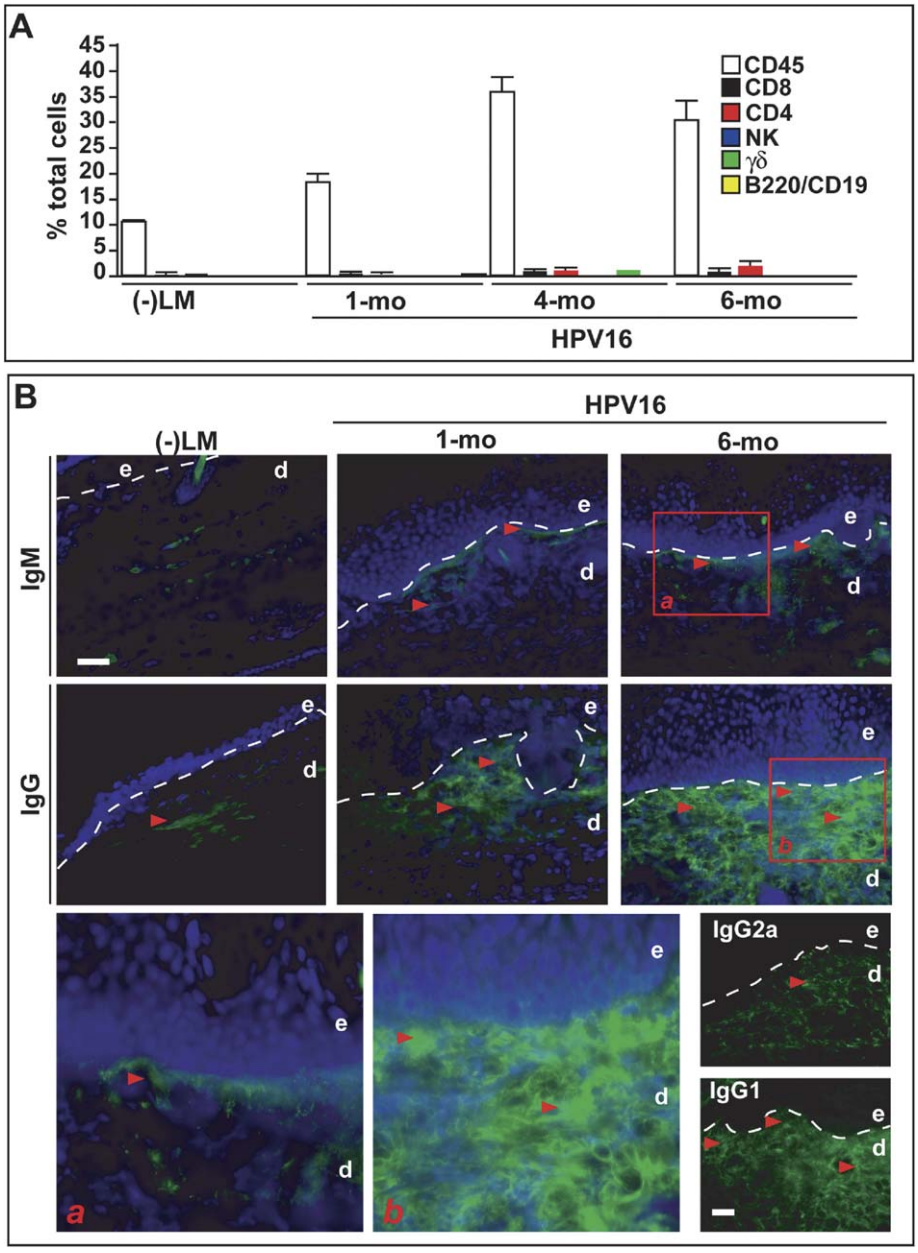

Figure 3. Immunoglobulin deposition characterizes *HPV16* premalignant skin

A: Percentages of $CD45^+$, $CD8^+$, $CD4^+$, $NK1.1^+$, $\gamma\delta TCR^+$, or $B220^+/CD19^+$ cells assessed by flow cytometry of (−)LM and *HPV16* ear tissue at 1, 4, and 6 months of age. Results shown are mean percentages (n = 5–7). Error bars represent SEM.
B: Direct immunofluorescence of IgM, IgG, IgG1, and IgG2a antibodies (arrowheads, green staining) and nuclei (blue) in skin of (−)LM and *HPV16* mice at 1 and 6 months of age. Dashed line, epidermal-dermal interface; epidermis, e; dermis, d. Scale bar, 50 μm. Boxed areas **A** and **B** are shown enlarged in lower left two panels.

tissue representing any premalignant stage (data not shown). Together, these data indicate that whereas B cells are not recruited into premalignant tissue, they are activated peripherally and initiate Ig deposition into neoplastic tissue paralleling chronic inflammation and premalignant progression in *HPV16* mice.

Adoptive transfer of B lymphocytes into *HPV16/RAG-1*$^{-/-}$ mice restores characteristics of premalignant progression

Based on the importance of B cells in regulating recruitment and activation of leukocytes during inflammation-associated pathologies and the abundant deposition of Ig in HPV16 skin (Figure 3B) coinciding with inflammatory cell infiltration, we hy-

Fluorescent angiography of premalignant *HPV16* and *HPV16/RAG-1*$^{-/-}$ skin (6 months of age). Scale bar, 100 μm.
C: Keratinocyte proliferation index in ears of (−)LM and premalignant *HPV16* and *HPV16/RAG-1*$^{-/-}$ mice at 1, 4, and 6 months of age. Values represent an average from five high-power fields per mouse, with 4 to 8 mice per category. Error bars represent SEM, and asterisk (*) indicates statistically significant differences between age-matched *HPV16* versus *HPV16/RAG-1*$^{-/-}$ mice ($p < 0.05$, Mann-Whitney).
D: Incidence of epithelial neoplasms in mice developing hyperplastic skin lesions by 1 month of age (Hyp), dysplasia by 6 months of age (Dys), dysplasia throughout lifetime, and lifetime incidence of SCCs. Values represent percentages of mice with particular neoplastic phenotypes.

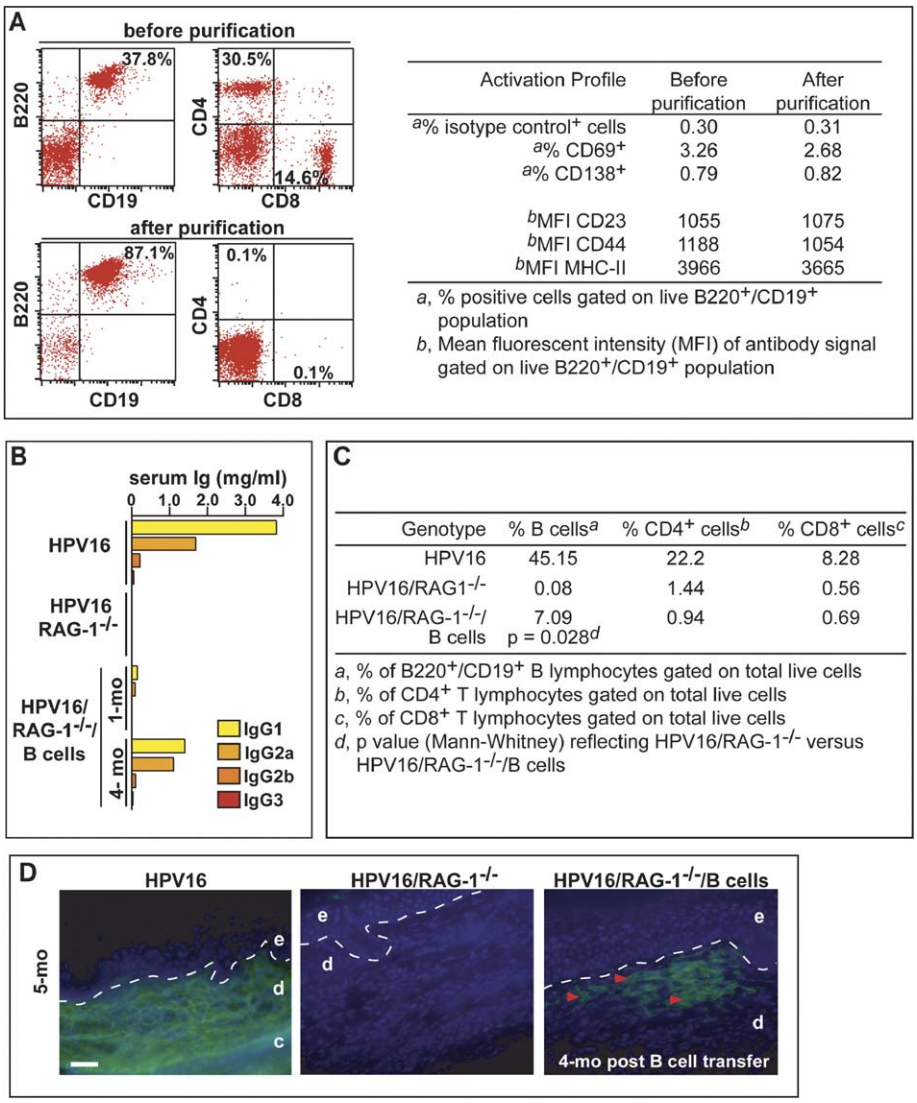

Activation Profile	Before purification	After purification
[a]% isotype control+ cells	0.30	0.31
[a]% CD69+	3.26	2.68
[a]% CD138+	0.79	0.82
[b]MFI CD23	1055	1075
[b]MFI CD44	1188	1054
[b]MFI MHC-II	3966	3665

a, % positive cells gated on live B220+/CD19+ population
b, Mean fluorescent intensity (MFI) of antibody signal gated on live B220+/CD19+ population

Genotype	% B cells[a]	% CD4+ cells[b]	% CD8+ cells[c]
HPV16	45.15	22.2	8.28
HPV16/RAG1-/-	0.08	1.44	0.56
HPV16/RAG-1-/-/ B cells	7.09 p = 0.028[d]	0.94	0.69

a, % of B220+/CD19+ B lymphocytes gated on total live cells
b, % of CD4+ T lymphocytes gated on total live cells
c, % of CD8+ T lymphocytes gated on total live cells
d, p value (Mann-Whitney) reflecting HPV16/RAG-1-/- versus HPV16/RAG-1-/-/B cells

Figure 4. Adoptive transfer of B cells into *HPV16/RAG-1*$^{-/-}$ mice results in antibody deposition in premalignant skin

A: Dot plots showing B (CD19+/B220+), CD4+, and CD8+ T cell percentages in spleens and lymph nodes from *HPV16* mice before and after B cell purification. Analysis of activation phenotypes of B220+/CD19+ B cells before and after enrichment by flow cytometry reveals percentages of CD69+ and CD138+ cells gated on live CD19+/B220+ B cells. Mean fluorescence intensity (MFI) of CD23, CD44, and MHC-II antibody signals of live B220+/CD19+ B cells are shown.

B: Ig levels determined by ELISA in serum from *HPV16* (4 months), *HPV16/RAG-1*$^{-/-}$ (4 months), and B cell reconstituted/*HPV16/RAG-1*$^{-/-}$ mice at indicated time points after adoptive transfer.

C: Percentages of B220+/CD19+ B cells, CD4+ T, and CD8+ T cells in spleens of *HPV16* (5 months), *HPV16/RAG-1*$^{-/-}$ (5 months), and B cell reconstituted *HPV16/RAG-1*$^{-/-}$ mice 4 months following adoptive transfer by flow cytometry.

D: Direct immunofluorescent detection of IgG (red arrowheads, green staining) in neoplastic skin of age-matched *HPV16*, *HPV16/RAG-1*$^{-/-}$, and B cell reconstituted/*HPV16/RAG-1*$^{-/-}$ mice, 4 months after reconstitution (5 months of age). Dashed line, epidermal-dermal interface; epidermis, e; dermis, d; cartilage, c; nuclei (blue staining). Scale bar, 50 μm.

pothesized that B cell deficiency in *HPV16/RAG-1*$^{-/-}$ mice was, in part, responsible for their attenuated neoplastic development. To assess this, we isolated B220+CD19+ B cells from spleens and lymph nodes of 3- to 6-month-old *HPV16* mice. At this age, *HPV16* mice have pronounced Ig deposition in skin and thus contain primed and/or memory B cells of desired specificity (Figure 4A). To exclude a potential activating effect of labeling B cells with antibodies, a negative purification procedure was applied by removing all non-B lymphocytes. The enriched population contained ~87% B220+CD19+ B cells, with the remainder composed predominantly of debris, a small fraction of NK1.1+ cells (<0.4%), γδ TCR+ cells (<2%), and <0.1% CD4+ and CD8+ T cells (data not shown and Figure 4A). This enrichment process did not select for subpopulations of (activated) B220+CD19+ B cells or alter the activation status of B220+CD19+ B cells as determined by flow cytometry (Figure 4A, right panel). Enriched B cell populations were adoptively transferred into 1-month-old *HPV16/RAG-1*$^{-/-}$ mice, and at specific time points post-transfer, serum was analyzed for Ig by ELISA (Figure 4B). Sera from B cell recipient-*HPV16/RAG-1*$^{-/-}$ mice exhibited detectable titers of Ig within 17 days, reached a stable level by 2 months of age, and remained at that level for at least 4 months (Figure 4B), indicating that adoptively transferred B cells survived and remained functional following transfer. Antibody titers in serum of B cell recipient-*HPV16/RAG-1*$^{-/-}$ mice were ~3-fold lower than in age-matched *HPV16* mice, an expected observation since only 7 × 10^6 B cells were transferred. T cell populations were not observed in lymphoid organs of B cell recipient-*HPV16/RAG-1*$^{-/-}$ mice (Figure 4C). Importantly, spatial depositions of Ig in skin of B cell recipient-*HPV16/RAG-1*$^{-/-}$ mice was similar, albeit less pronounced, to age-matched *HPV16* mice where patches of IgG were detectable in dermal stroma 1 month following B cell transfer (data not shown) that became more pronounced with age (Figure 4D).

We next investigated whether adoptive transfer of B cells into *HPV16/RAG-1*$^{-/-}$ mice restored characteristic parameters of premalignancy and found that B cell recipient/*HPV16/RAG-1*$^{-/-}$ mice exhibited characteristic infiltration of CD45+ leukocytes (Figure 5A) and abundant presence of MCs and

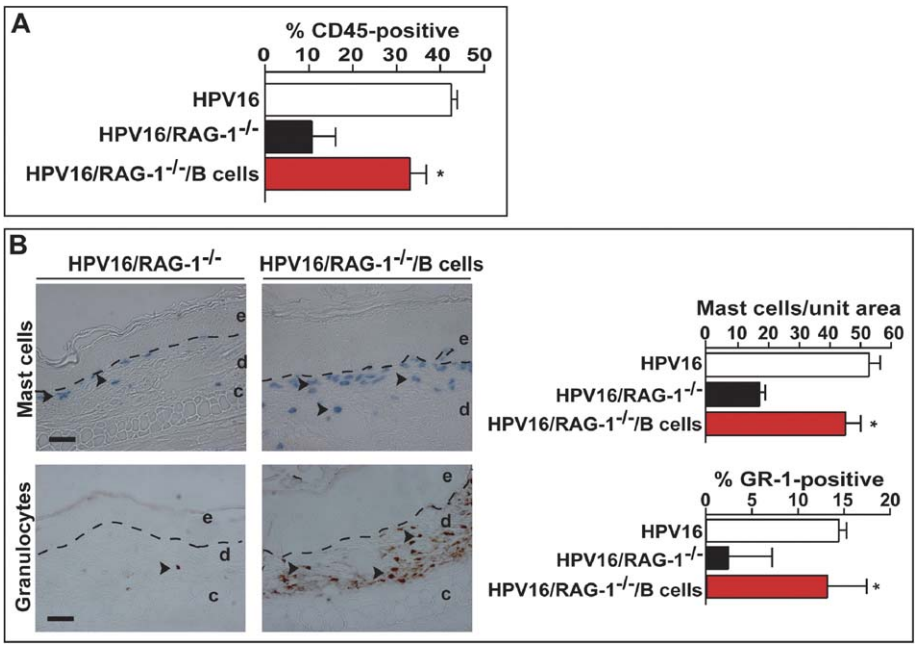

Figure 5. Adoptive transfer of B cells into *HPV16/RAG-1*$^{-/-}$ mice restores inflammation in premalignant skin

A: Percentages of CD45^{+} cells in age-matched skin from *HPV16*, *HPV16/RAG-1*$^{-/-}$, and B cell reconstituted *HPV16/RAG-1*$^{-/-}$ mice (4 months after B cell transfer) analyzed by flow cytometry. Error bars represent SEM, and asterisk (*) indicates statistically significant differences between age-matched *HPV16/RAG-1*$^{-/-}$ versus B cell recipient *HPV16/RAG-1*$^{-/-}$ mice ($p < 0.05$, unpaired t test).

B: Mast cells (blue staining cells, arrowheads, upper panels) and granulocytes (brown staining cells, arrowheads, lower panels) in ear tissue of age-matched *HPV16/RAG-1*$^{-/-}$ and B cell reconstituted/*HPV16/RAG-1*$^{-/-}$ mice (4 months after B cell transfer). Dashed line, epidermal-dermal interface; epidermis, e; dermis, d; cartilage, c. Graphical representation of mast cell numbers averaged from five high-power fields per mouse and four mice per category. Percentage of GR-1^{+} cells analyzed by flow cytometry of age-matched ear tissue of *HPV16*, *HPV16/RAG-1*$^{-/-}$, and B cell reconstituted *HPV16/RAG-1*$^{-/-}$ ear skin (4 months after B cell transfer). Error bars represent SEM, and asterisk (*) indicates statistically significant differences between age-matched *HPV16/RAG-1*$^{-/-}$ versus B cell recipient *HPV16/RAG-1*$^{-/-}$ mice ($p < 0.05$, Mann-Whitney).

granulocytes in dermal stroma (Figure 5B), suggesting that B cells play a crucial role in regulating chronic inflammation associated with premalignant progression in *HPV16* mice. Moreover, neoplastic skin of B cell recipient-*HPV16/RAG-1*$^{-/-}$ mice exhibited restored characteristic parameters of premalignancy downstream of chronic inflammation, e.g., development of angiogenic vasculature and keratinocyte hyperproliferation (Figures 6A and 6B). Taken together, these data indicate that B cells are critical adaptive immune cells necessary for innate immune cell infiltration, activation, and responses downstream of oncogene expression in neoplastic skin.

Transfer of serum from *HPV16* mice into *HPV16/RAG-1*$^{-/-}$ mice restores premalignant characteristics

Since abundant Ig deposition in dermal stroma is characteristic of *HPV16* premalignancy (Figure 3), we hypothesized that B cells exert their effect via production of antibodies or other soluble factors in serum. To assess this, we transferred serum from 3- to 6-month-old *HPV16* mice at weekly intervals into *HPV16/RAG-1*$^{-/-}$ mice starting at 1 month of age and continuing for 4 months. After 4 months, we found Ig in *HPV16/RAG-1*$^{-/-}$ skin whose spatial deposition was similar, albeit less pronounced, to age-matched *HPV16* mice (Figure 7A). Importantly, transfer of *HPV16* serum into *HPV16/RAG-1*$^{-/-}$ mice restored infiltration of CD45^{+} cells (Figure 7B) as well as increased infiltration of MCs and granulocytes as compared to age-matched *HPV16/RAG-1*$^{-/-}$ mice (Figure 7C), suggesting that serum factors in *HPV16* mice play a role in regulating chronic inflammation associated with premalignant progression. Moreover, premalignant skin of serum transferred-*HPV16/RAG-1*$^{-/-}$ mice exhibited enhanced development of angiogenic vasculature and keratinocyte hyperproliferation as compared to age-matched *HPV16/RAG-1*$^{-/-}$ mice (Figures 7D and 7E), similar to that observed following B cell transfer (Figure 6). To determine the specificity of serum rescue, we transferred serum from nontransgenic mice into 1-month-old *HPV16/RAG-1*$^{-/-}$ mice and found no change in phenotype as assessed by Ig deposition, leukocyte infiltration, or vascular architecture (unpublished data). Taken together, these data indicate that peripheral B cell responses in *HPV16* mice mediate innate immune cell infiltration, activation, and responses downstream of oncogene expression in neoplastic skin via production of mediators found in serum.

Discussion

It is well established that chronic inflammation contributes to cancer development (Balkwill et al., 2005; Coussens and Werb, 2002). It is not clear, however, which mechanisms are responsible for initiation and/or maintenance of chronic inflammation associated with developing neoplasms. This study revealed a provocative new insight into the role of adaptive immunity, specifically B cells, as important regulators of inflammation-associated cancer development. Using a transgenic mouse model of multistage epithelial carcinogenesis, e.g., *HPV16* mice, we found that genetic deletion of adaptive immune cells resulted in attenuated recruitment of innate immune cells toward premalignant skin. As a consequence, tissue remodeling, angiogenesis, and epithelial hyperproliferation were significantly reduced, culminating in reduced carcinoma incidence. Importantly, transfer of B cells or serum from *HPV16* mice into T and B lymphocyte-deficient/*HPV16* mice resulted in restored Ig deposition in premalignant skin, recruitment of leukocytes, and characteristic parameters of premalignancy. Together,

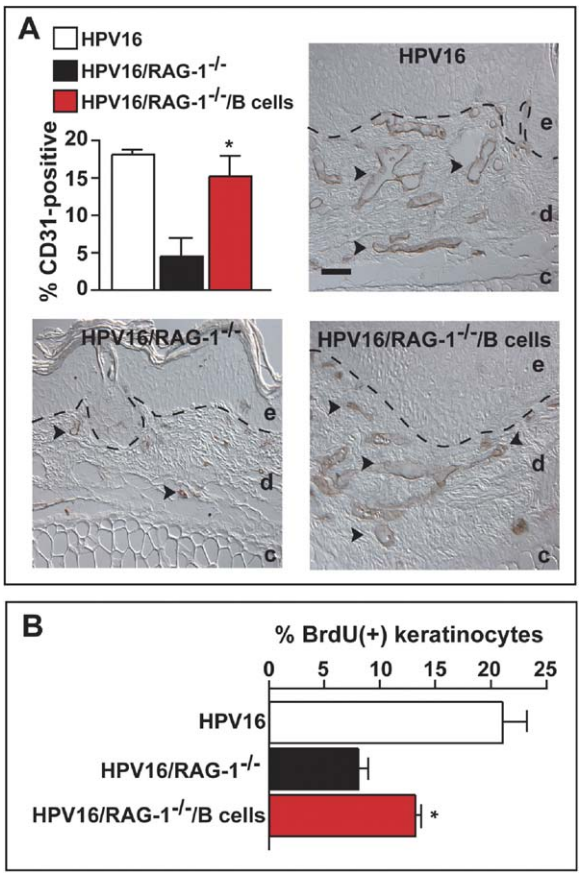

Figure 6. Adoptive transfer of B cells from *HPV16* mice into *HPV16/RAG-1*$^{-/-}$ mice restores characteristics of premalignant progression

A: Percentage of CD31^{+} cells analyzed by flow cytometry from single-cell suspensions of age-matched *HPV16*, *HPV16/RAG-1*$^{-/-}$, and B cell reconstituted/*HPV16/RAG-1*$^{-/-}$ ears (4 months after B cell transfer). Error bars represent SEM, and asterisk (*) indicates statistically significant differences between age-matched *HPV16/RAG-1*$^{-/-}$ versus B cell recipient/*HPV16/RAG-1*$^{-/-}$ mice ($p < 0.05$, unpaired t test). Immunolocalization of CD31 (arrowheads, brown staining) in age-matched ear tissue of *HPV16*, *HPV16/RAG-1*$^{-/-}$, and B cell recipient/*HPV16/RAG-1*$^{-/-}$ mice (4 months after adoptive transfer). Dashed line, epidermal-dermal interface; epidermis, e; dermis, d; cartilage, c. Scale bar, 50 μm.

B: Keratinocyte proliferation index in ear tissue of *HPV16*, *HPV16/RAG-1*$^{-/-}$, and B cell reconstituted/*HPV16/RAG-1*$^{-/-}$ mice (4 months after adoptive transfer). Values reflect averages from five high-power fields per mouse, four mice per category. Error bars represent SEM, and asterisk (*) indicates statistically significant differences between age-matched *HPV16/RAG1*$^{-/-}$ versus B cell recipient/*HPV16/RAG-1*$^{-/-}$ mice ($p < 0.05$, Mann-Whitney).

these data indicate that peripheral B cell activation is an essential step for early epithelial neoplastic development, and B cell-derived soluble mediators are necessary for establishing chronic inflammatory states that potentiate malignant progression.

B lymphocytes mediate chronic inflammation

B lymphocytes do not infiltrate premalignant skin in *HPV16* mice, suggesting that they play an immunomodulatory role in a paracrine manner following interactions with Langerhans or dendritic cells presenting skin-derived antigens in draining lymph nodes and/or spleen. Moreover, since transfer of serum from *HPV16* mice reinstates characteristics of neoplastic progression to *HPV16/RAG-1*$^{-/-}$ mice similar to that observed following adoptive transfer of B cells (isolated from *HPV16* mice), we propose that B lymphocytes exert their effect distally via production of soluble mediators that enter the circulation and home to premalignant tissues.

What types of serum-derived soluble mediators produced distally by activated B cells could underlie activation and maintenance of chronic inflammation in *HPV16* mice? Activated B cells may regulate chronic inflammation and cancer development via altering circulating cytokine and/or chemokine profiles/levels. Depending on the scenario, it has been reported that activated B cells produce CXCL1 chemokines (KC and MIP-2), IL-4, IL-6, and IL-10 (Hu et al., 2004; Lenert et al., 2005; Sato et al., 2004; Viau and Zouali, 2005). These chemokines and cytokines have been implicated in modulating innate immunity during pathogenic and/or acute states of inflammation (Balkwill et al., 2005) and may thus also be involved in mediating recruitment of leukocytes to neoplastic skin.

Another mechanism whereby B cells are known to exert immunomodulatory effects is via antibody production (Viau and Zouali, 2005). There is ample evidence that Ig-mediated pathways participate in the pathogenesis of experimental and clinical inflammatory disorders (Lee et al., 2002; Liu et al., 1993; Sylvestre and Ravetch, 1996). Mechanisms for this participation involve Ig-antigen complex formation and subsequent activation of complement cascades resulting in formation and liberation of anaphylatoxins, e.g., C3a and C5a, potent proinflammatory factors that induce recruitment and activation of leukocytes (Hartmann et al., 1997). Alternatively, antibodies could activate innate immune cells via direct engagement with antibody binding multimeric cell surface Fc receptors (FcR) (Clynes and Ravetch, 1995).

Premalignant *HPV16* skin is characterized by abundant Ig deposition (absent in *HPV16/RAG-1*$^{-/-}$ mice, but restored following transfer of serum isolated from *HPV16* mice but not nontransgenic mice); thus, once in the neoplastic microenvironment, antibodies could mediate recruitment of innate immune cells via activation of complement cascades or engagement of FcR expressed on resident immune cells. Depositions of complement component C3 are present in *HPV16/RAG-1*$^{-/-}$ skin (Figure S2 in the Supplemental Data available with this article online), indicating that the complement system alone is not sufficient for induction of chronic inflammation during neoplastic progression. Taken together with the fact that C3-deficient/*HPV16* mice display characteristic antibody deposition, chronic inflammation, angiogenesis, and keratinocyte hyperproliferation (de Visser et al., 2004), we speculated that antibodies produced distally by activated B cells home to neoplastic skin and modulate chronic inflammation by cross-linking FcR on resident leukocytes, resulting in an initial "trigger" inducing rapid degranulation and release of proinflammatory mediators that further enhance the cascade of activation and recruitment of innate immune cells. To distinguish between the functional significance of antibodies versus other soluble mediators present in serum, we are currently performing transfer experiments with purified Igs isolated from *HPV16* mice.

This report demonstrates that spontaneous activation of B cells promotes de novo epithelial carcinogenesis by initiating chronic inflammation. A link between B cells, antibodies, and cancer development has been postulated previously, based on

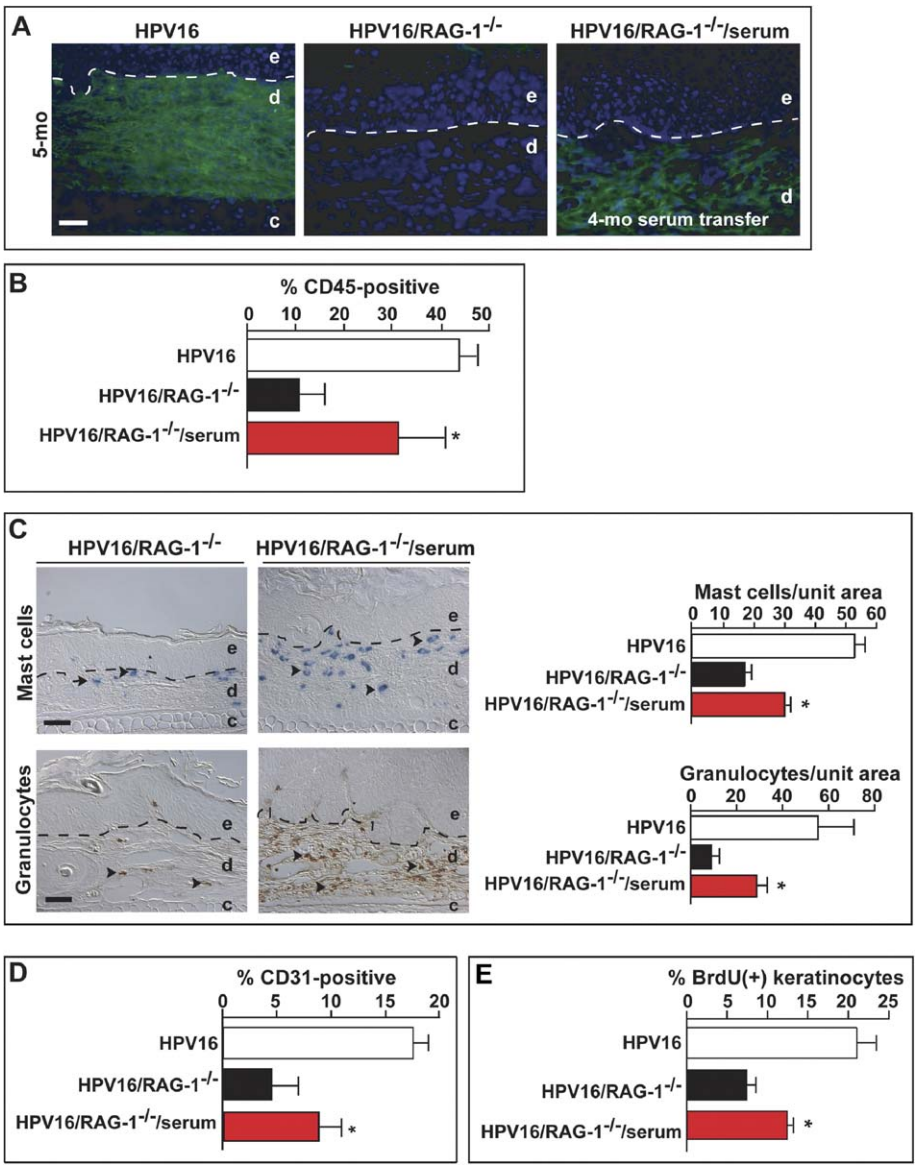

Figure 7. Transfer of serum from *HPV16* mice into *HPV16/RAG-1*$^{-/-}$ mice enhances premalignant progression

A: Direct immunofluorescent detection of IgG antibodies (green staining) and nuclei (blue staining) in neoplastic skin of age-matched *HPV16*, *HPV16/RAG-1*$^{-/-}$, and *HPV16/RAG-1*$^{-/-}$ mice injected with *HPV16* serum at weekly intervals for 4 months (5 months of age). Dashed line, epidermal-dermal; epidermis, e; dermis, d; cartilage, c. Scale bar, 50 μm.

B: Percentage of CD45^{+} cells determined by flow cytometry in age-matched *HPV16*, *HPV16/RAG-1*$^{-/-}$, and serum transferred/HPV/*RAG-1*$^{-/-}$ mice (4 months after initiation of serum transfer). Error bars represent SEM, and asterisk (*) indicates statistically significant differences between age-matched *HPV16/RAG-1*$^{-/-}$ versus serum transferred/*HPV16/RAG-1*$^{-/-}$ mice ($p < 0.05$, Mann-Whitney).

C: Mast cells (blue staining, arrowheads, upper panels) and granulocytes (brown staining, arrowheads, lower panels) in ear tissue of age-matched *HPV16/RAG-1*$^{-/-}$ and serum transferred/*HPV/RAG-1*$^{-/-}$ mice (4 months after initiation of serum transfer). Dashed line, epidermal-dermal interface; epidermis, e; dermis, d; cartilage, c. Scale bar, 50 μm. Values reflect averages from five high-power fields per mouse and 3 to 7 mice per category. Error bars represent SEM, and asterisk (*) indicates statistically significant differences between age-matched *HPV16/RAG-1*$^{-/-}$ versus serum transferred/*HPV16/RAG-1*$^{-/-}$ mice ($p < 0.05$, Mann-Whitney).

D: Percentage of CD31^{+} cells analyzed by flow cytometry in ear tissue from *HPV16*, *HPV16/RAG-1*$^{-/-}$, and serum transferred/*HPV16/RAG-1*$^{-/-}$ mice (4 months after initiation of serum transfer). Error bars represent SEM, and asterisk (*) indicates statistically significant differences between age-matched *HPV16/RAG-1*$^{-/-}$ versus serum transferred/*HPV16/RAG-1*$^{-/-}$ mice ($p < 0.05$, Mann-Whitney).

E: Keratinocyte proliferation index in ear tissue of *HPV16*, *HPV16/RAG-1*$^{-/-}$, and serum transferred/*HPV16/RAG-1*$^{-/-}$ mice (4 months after initiation serum transfer). Values reflect averages from five high-power fields per mouse (n = 3–7). Error bars represent SEM, and asterisk (*) indicates statistically significant differences between age-matched *HPV16/RAG1*$^{-/-}$ versus serum transferred/*HPV16/RAG-1*$^{-/-}$ mice ($p < 0.05$, Mann-Whitney).

observations that low antibody responder mice are more resistant to tumor induction by carcinogens (Ibanez et al., 1999). In addition, passive transfer or actively produced antibodies following vaccination enhance in vivo outgrowth of injected tumor cells (Ishibashi et al., 1978; Nyhus et al., 2001). Moreover, active immunization of mice carrying a mutant *ras* oncogene results in activation of humoral immune responses and enhanced papilloma formation upon chemical promotion (Schreiber et al., 2000; Siegel et al., 2000). Other studies have reported that antitumor humoral immune responses potentiate in vivo growth and invasion of injected murine and human tumor cell lines via recruitment and activation of granulocytes and macrophages (Barbera-Guillem et al., 1999; Barbera-Guillem et al., 2002). Whether these observations are unique for tumor transplantation where premalignant progression is circumvented or whether de novo carcinogenesis follows similar scenarios was not addressed. In combination with these previous observations, our data support a role for B cells as important contributors to the earliest steps of neoplastic progression by regulating chronic inflammation in premalignant tissues.

Activation of B lymphocytes during premalignant progression

B lymphocytes responsible for initiating chronic inflammation in *HPV16* skin could be specific for several types of antigens, e.g., pathogen-derived antigens, neo-antigens, or self-antigens. Several types of human malignancies are associated with chronic inflammation as a consequence of bacterial infections, i.e., *Helicobacter pylori* infection results in chronic inflammation and predisposes to gastric carcinoma (Ernst and Gold,

2000). Similarly, chronic colon inflammation caused by bacteria, viruses, or irritants predisposes to colon carcinogenesis (Shacter and Weitzman, 2002). These clinical observations suggest a correlation between induction of inflammatory reactions following pathogen or irritant exposure and neoplastic risk; however, a critical role for B cells has thus far not been reported. To address the significance of bacterial antigens as activators of B cell responses and chronic inflammation in *HPV16* mice, we generated a colony of germ-free *HPV16* mice. Analysis of this colony indicates that the relative contribution of bacterial-specific antigens is minimal (K.E.d.V. et al., unpublished data). Alternatively, B cell responses may be directed toward neo-antigens, e.g., antigens only present in neoplastic tissue as a consequence of genetic alteration and expression of mutant protein, or self-antigens derived from proteins undergoing neoplasia-specific tissue remodeling and generation of cryptic epitopes. Based on the fact that Ig deposits in *HPV16* skin are limited to dermal stroma (Figure 3B), we anticipate that corresponding antigens derive from ECM proteins undergoing remodeling in the surrounding stroma. Interestingly, the immunological events occurring during premalignancy in *HPV16* mice have striking similarities with various experimental and human autoimmune disorders. For example, in patients with epidermolysis bullosa acquisitia and bullous pemphigoid, deposits of self-specific antibodies are observed in the dermis along basement membranes (Schaumburg-Lever et al., 1975; Woodley et al., 1984). Similar to our observations in *HPV16* mice, in experimental models of bullous pemphigoid and arthritis, deposition of self-specific antibodies results in recruitment of MCs and neutrophils prior to blister formation or arthritis (Chen et al., 2002; Lee et al., 2002). Whether B cell responses mediating chronic inflammation in premalignant *HPV16* skin are reactive toward self-antigens remains to be established. The observation that circulating self-specific antibodies against HPV16 E7 are detected in *HPV16* mice suggests that premalignant progression does involve autoantibody formation (Daniel et al., 2003), the significance of which, with regard to chronic inflammation, remains to be determined.

Involvement of T lymphocytes

To ensure that adoptively transferred B cells contained primed and memory B cells capable of secreting Ig that homed to neoplastic skin, we isolated B lymphocytes from spleens and lymph nodes of 3- to 6-month-old *HPV16* mice (Figure 4). Previous studies demonstrated that memory B cells adoptively transferred into *RAG-1*$^{-/-}$ mice maintained the ability to secrete antibodies in the absence of T cell help (Hebeis et al., 2004). When we evaluated *HPV16/CD4*$^{-/-}$*/CD8*$^{-/-}$ mice, we found characteristic Ig deposition and infiltration of innate immune cells in premalignant skin (data not shown and Figure 1), suggesting that B cell responses may be independent of mature CD4$^+$ and CD8$^+$ T cells. A caveat to this is that while *CD4*$^{-/-}$/*CD8*$^{-/-}$ mice indeed lack CD4 and CD8α coreceptors, a small residual population of T lymphocytes may be present and involved in priming B lymphocytes (Locksley et al., 1993; Schilham et al., 1993). Further studies are needed to address the exact role of T cells in the induction of tumor-enhancing B cell responses.

It has previously been reported that CD4$^+$ T cells regulate carcinoma latency in *HPV16* mice via altering the presence of CD11b$^+$ and Gr-1$^+$ immune cells in fully dysplastic skin (Daniel et al., 2003). When we evaluated premalignant *HPV16/CD4*$^{-/-}$ and *HPV16/CD4*$^{-/-}$*/CD8*$^{-/-}$ tissues, we did not observe reduced percentages of CD45$^+$, GR-1$^+$, or mast cells as compared to the dramatic reductions found in age-matched *HPV16/RAG-1*$^{-/-}$ mice (Figure 1). Thus, our data indicate that B cells are critical for establishing initial regulatory circuits leading to chronic innate immune cell infiltration during the earliest stages of premalignant progression, and when absent, results in significantly reduced premalignant progression and carcinoma development. In contrast, CD4$^+$ T lymphocytes do not appear to regulate establishment of chronic inflammation, but instead affect late-stage presence of innate immune cells and modestly alter carcinoma latency (Daniel et al., 2003).

Adaptive immunity and cancer development: implications

A prevalent view of the relationship between adaptive immunity and cancer is that adaptive immune cells exert a protective role against developing neoplasms, i.e., immune surveillance (Dunn et al., 2002), the existence of which remains a matter of debate (Qin and Blankenstein, 2004). In this study, we report that genetic elimination of mature B and T cells does not enhance premalignant progression or carcinoma incidence, but rather reduces it. These data are in contrast to epidemiological studies of immunodeficient or immunosuppressed humans who demonstrate increased risk of certain types of neoplasms, including nonmelanoma skin cancer (Boshoff and Weiss, 2002). This paradox is most logically explained by differences in cancer etiology between immunocompromised patients versus *HPV16/RAG-1*$^{-/-}$ mice, where in the former, malignancies typically arise due to viral infection, e.g., HPV16-related cervical and squamous carcinomas, Epstein-Barr virus-related non-Hodgkin's lymphoma, and Kaposi's sarcoma associated with human herpesvirus 8 (Boshoff and Weiss, 2002). The relatively high incidence of these malignancies in immunocompromised patients can at least partially be explained by their increased susceptibility to viral infection and/or viral reactivation. In this report, however, we analyzed the role of adaptive immunity during premalignant progression in transgenic mice harboring viral oncoproteins as opposed to virus-infected mice. Consistent with our observations regarding absence of immune surveillance during premalignant progression in *HPV16* mice, in human immunodeficiency virus-positive patients, incidence of the most prevalent epithelial cancer types of nonviral etiology, e.g., colon, prostate, breast, and ovarian, are similarly reduced (Boshoff and Weiss, 2002).

Our data implicating B lymphocytes as enhancers of premalignancy by potentiating chronic inflammation suggest that passive transfer antibody therapies and active immunotherapeutical approaches may have disparate outcomes when antibody responses are induced against solid malignancies as opposed to premalignant disease. The possibility of potentiating malignant risk by activating humoral B cell responses is underscored by our data (Figure 7) and other studies reporting enhanced neoplastic progression and tumor growth following passively transferred or actively produced antibodies (Barbera-Guillem et al., 2000; Nyhus et al., 2001; Siegel et al., 2000). These data suggest that enhanced neoplastic risk may follow vaccination modalities in cancer-prone patients or patients with premalignant disease via inadvertently inducing humoral immune responses. That said, potential enhancement of chronic tumor-promoting host responses could be circum-

vented by the use of specifically engineered antibodies lacking functional Fc domains that fail to interact with and/or stimulate resident inflammatory cells.

In conclusion, data reported herein support a model in which the adaptive immune system functionally interacts with the innate immune system and that both components are critically involved during the early stages of neoplastic progression. In addition, this study suggests that pharmacological interventions attenuating B cell activation or blocking B cell-mediated recruitment of innate immune cells may be effective in preventing premalignant epithelial progression.

Experimental Procedures

Transgenic mice and histopathologic analyses

Generation and characterization of *HPV16* mice and mice homozygous null (–/–) for *RAG-1* and *CD4* and *CD8α* coreceptors have been described previously (Chen et al., 1994; Coussens et al., 1996; Mombaerts et al., 1992; Rahemtulla et al., 1991). To generate *HPV16* mice in the *RAG-1*$^{-/-}$, *CD4*$^{-/-}$, and *CD8*$^{-/-}$ backgrounds, *RAG-1*$^{+/-}$, *CD4*$^{+/-}$, and *CD8*$^{+/-}$ mice were backcrossed into the FVB/n strain to N15, N14, and N6, respectively, where they were then intercrossed with *HPV16* mice to generate breeding colonies of *HPV16/RAG-1*$^{-/-}$, *HPV16/CD4*$^{-/-}$, *HPV16/CD8*$^{-/-}$, and *HPV16/CD4*$^{-/-}$/*CD8*$^{-/-}$ mice. All mice were maintained within the UCSF Laboratory for Animal Care barrier facility according to IACUC procedures. Characterization of neoplastic stages based on hematoxylin and eosin staining and keratin intermediate filament expression for histologic examination have been reported previously (Coussens et al., 1996; Daniel et al., 2003).

Flow cytometry

Single-cell suspensions were prepared from ears of negative littermate [(–)LM] and transgenic mice as described previously (de Visser et al., 2004). Cells were incubated for 10 min at 4°C with rat anti-mouse CD16/CD32 mAb (BD Biosciences, San Diego, CA) at a 1:100 dilution in PBS/BSA to prevent nonspecific antibody binding. Subsequently, cells were washed and incubated for 20 min with 50 μl of 1:100 dilution of primary antibody followed by two washes with PBS/BSA. 7-AAD (BD Biosciences) was added (1:10) to discriminate between viable and dead cells. Data acquisition and analysis were performed on a FACSCalibur using CellQuestPro software (BD Biosciences). Data shown represent mean ± SEM. See the Supplemental Data section for specifics on primary antibody use.

Enzyme- and immunohistochemistry

Immunohistochemical (IHC) detection and chloroacetate esterase (CAE) histochemistry was performed as previously described (Coussens et al., 1996; Coussens et al., 1999; Coussens et al., 2000; de Visser et al., 2004). All immunolocalization experiments were repeated on multiple tissue sections and included negative controls for determination of background staining, which was negligible. Data shown are representative of results obtained following examination of tissues removed from a minimum of five different mice per time point. Quantitative analysis of MCs and granulocytes was performed by counting cells in five high-power fields (40×) per age-matched tissue section from five mice per group. Data presented reflect the mean total cell count per field from the ventral ear leaflet.

Fluorescent angiography

Anesthetized mice were injected i.v. with 0.05 mg FITC-labeled tomato lectin (*Lycopersicon esculentum*; Vector) and analyzed using a laser-scanning confocal Zeiss LSM510 META microscope with a Zeiss LSM Image Examiner as previously described (van Kempen et al., 2002).

Gelatinase solution assay

Protein lysates were prepared for enzyme solution assays as previously described (Rhee et al., 2004). Fluorescence was measured (excitation 485 nm, emission 530 nm) on a SpectraMax Gemini spectrophotometer (Molecular Devices, Sunnyvale, CA) operated by SoftMax Pro 4.3 software (Molecular Devices). Metalloproteinase inhibition was performed in the presence of 4.0 mM 1,10-phenanthroline (Sigma, St. Louis, MO). Change in relative fluoresence units (RFU)/min/μg tissue protein was determined using SoftMax Pro 4.3 software (Molecular Devices).

Substrate zymography

Fresh-frozen ears from (–)LM or transgenic mice were weighed, and protein lysates were prepared for gelatin substrate zymography as previously described (Coussens et al., 2000; Rhee et al., 2004).

ELISA

VEGF-A ELISA

Tissue lysates were prepared as described above for substrate zymography. VEGF-A levels in tissue lysates were assayed using the quantikine mouse VEGF-A immunoassay kit (R&D systems, Minneapolis, MN) as described by the manufacturer, using 50 μg of protein. Optical density was measured at 450 nm with wavelength correction set to 540 nm on a SpectraMax 340 spectrophotomoter (Molecular Devices). Antibody concentrations were calculated using SoftMax Pro 4.1 (Molecular Devices).

Immunoglobulin ELISA

Serum ELISA to analyze Ig levels was performed as described by the manufacturer's recommendations using the clonotyping system-HRP kit (SouthernBiotech, Birmingham AL). Optical density was measured at 405 nm on a SpectraMax 340 spectrophotomoter (Molecular Devices, Sunnyvale, CA). Samples were assayed from at least four mice per category. Ig concentrations were calculated using SoftMax Pro 4.1 (Molecular Devices).

Immunofluorescence detection of immunoglobulin deposition

Immunofluorescent detection of immunoglobulin subtypes was performed essentially as described (de Visser et al., 2004). Data shown are representative of results obtained following examination of tissues removed from a minimum of four mice per category. All IF experiments included negative controls for determination of background staining that was negligible. Specific details on antibodies used are provided in Supplemental Data.

Adoptive transfer of B lymphocytes

Spleen and lymph nodes from *HPV16* mice (3–6 months of age) were homogenized through a 70 μm nylon filter (Falcon). Single-cell suspensions were treated with 1xPharM Lyse ammonium chloride lysing reagent (BD Biosciences) for 5 min to remove erythrocytes. Cells were washed with DMEM containing 5% FBS and were enriched for viable lymphocytes over a Lympholyte-M gradient (Cedarlane Laboratories, Hornby, Ontario, Canada). Cells were washed with DMEM 5% FBS, followed by a wash with PBS containing 1% FBS. To exclude a potential activating effect of labeling B cells with antibodies, a negative purification procedure was applied by removing all non-B lymphocytes using the Mouse B Cell Recovery Column Kit (Cedarlane). Briefly, 1×10^8 cells were incubated with antibody cocktail for 1 hr on ice. Antibody-labeled cells were removed by affinity chromatography using immunocolumns containing agarose beads. Eluted cells were washed with PBS, and purity of the B cell population confirmed by flow cytometry using APC-anti-CD19, FITC-anti-B220, PE-anti-CD8, FITC-anti-CD4, FITC-anti-γδ TCR, and FITC-anti-NK1.1 (1:100; eBioscience). Percentages of CD4$^+$ and CD8$^+$ T cells were <0.1%, γδ TCR$^+$ cells were <2%, and NK1.1$^+$ cells <0.4% of the total. In addition, we confirmed that the enrichment process did not result in activation of B cells and/or select for a subset of activated B lymphocytes by comparing activation phenotypes before and after the enrichment procedure by flow cytometry using PE-anti-CD44, PE-anti-CD23, PE-anti-MHC-II, PE-anti-CD69, and PE-anti-CD138 (1:100; BD Biosciences). 7×10^6 B cells were adoptively transferred into 1-month-old *HPV16/RAG-1*$^{-/-}$ mice in 200 μl PBS by tail vein injection. For in vivo depletion of potentially contaminating CD4$^+$ T cells after adoptive transfer, mice were injected twice (on the day of transfer and 1 day after transfer) with 200 μg each of purified GK1.5 antibody.

Serum transfer

Serum pools were prepared from *HPV16* or wild-type FVB/n mice at 3–6 months of age. Serum was transferred into *HPV16/RAG-1*$^{-/-}$ mice by i.p. injection of 200 μl serum at weekly intervals. Serum transfer into *HPV16/RAG-1*$^{-/-}$ mice was started at 1 month of age and continued for 4 months.

Statistical analyses

Statistical analyses were performed using GraphPad Prism version 4 and/or InStat version 3.0a for Macintosh (GraphPad Software, San Diego, CA).

Specific tests used were Mann-Whitney (unpaired, nonparametric, two-tailed), unpaired t test Welch corrected, Fishers exact test, and Log rank analysis. p values < 0.05 were considered statistically significant.

Supplemental Data

The Supplemental Data for this article, including Supplemental Experimental Procedures and Figures, can be found at http://www.cancercell.org/cgi/content/full/7/5/411/DC1/.

Acknowledgments

We thank members of the Coussens laboratory for insightful discussions, Drs. A. Eichten and S. Robinson for assistance with VEGF ELISA and FACS analyses, Dr. D. Hanahan for initially providing breeding colonies of *RAG-1*, *CD4*, and *CD8*-deficient mice and for helpful discussions, Dr. L. Lanier for critically reading the manuscript, Dr. D. Daniel for useful suggestions, and Eva Soliven, William Hyun, and Sarah Elmes for technical assistance. K.E.d.V. is supported by a fellowship from the Dutch Cancer Society. L.M.C. is supported by grants from the NIH, NCI, and Department of Army, BCCOE.

Received: December 8, 2004
Revised: February 25, 2005
Accepted: April 13, 2005
Published: May 16, 2005

References

Arbeit, J.M., Munger, K., Howley, P.M., and Hanahan, D. (1994). Progressive squamous epithelial neoplasia in K14-human papillomavirus type 16 transgenic mice. J. Virol. *68*, 4358–4368.

Balkwill, F., Charles, K.A., and Mantovani, A. (2005). Smoldering and polarized inflammation in the initiation and promotion of malignant disease. Cancer Cell *7*, 211–217.

Barbera-Guillem, E., May, K.F., Jr., Nyhus, J.K., and Nelson, M.B. (1999). Promotion of tumor invasion by cooperation of granulocytes and macrophages activated by anti-tumor antibodies. Neoplasia *1*, 453–460.

Barbera-Guillem, E., Nelson, M.B., Barr, B., Nyhus, J.K., May, K.F., Jr., Feng, L., and Sampsel, J.W. (2000). B lymphocyte pathology in human colorectal cancer. Experimental and clinical therapeutic effects of partial B cell depletion. Cancer Immunol. Immunother. *48*, 541–549.

Barbera-Guillem, E., Nyhus, J.K., Wolford, C.C., Friece, C.R., and Sampsel, J.W. (2002). Vascular endothelial growth factor secretion by tumor-infiltrating macrophages essentially supports tumor angiogenesis, and IgG immune complexes potentiate the process. Cancer Res. *62*, 7042–7049.

Bergers, G., and Coussens, L.M. (2000). Extrinsic regulators of epithelial tumor progression: metalloproteinases. Curr. Opin. Genet. Dev. *10*, 120–127.

Bergers, G., Brekken, R., McMahon, G., Vu, T.H., Itoh, T., Tamaki, K., Tanzawa, K., Thorpe, P., Itohara, S., Werb, Z., and Hanahan, D. (2000). Matrix metalloproteinase-9 triggers the angiogenic switch during carcinogenesis. Nat. Cell Biol. *2*, 737–744.

Bissell, M.J., and Radisky, D. (2001). Putting tumours in context. Nat. Rev. Cancer *1*, 46–54.

Boshoff, C., and Weiss, R. (2002). AIDS-related malignancies. Nat. Rev. Cancer *2*, 373–382.

Chen, J., Shinkai, Y., Young, F., and Alt, F.W. (1994). Probing immune functions in RAG-deficient mice. Curr. Opin. Immunol. *6*, 313–319.

Chen, R., Fairley, J.A., Zhao, M.L., Giudice, G.J., Zillikens, D., Diaz, L.A., and Liu, Z. (2002). Macrophages, but not T and B lymphocytes, are critical for subepidermal blister formation in experimental bullous pemphigoid: macrophage-mediated neutrophil infiltration depends on mast cell activation. J. Immunol. *169*, 3987–3992.

Clynes, R., and Ravetch, J.V. (1995). Cytotoxic antibodies trigger inflammation through Fc receptors. Immunity *3*, 21–26.

Coussens, L.M., and Werb, Z. (2002). Inflammation and cancer. Nature *420*, 860–867.

Coussens, L.M., Hanahan, D., and Arbeit, J.M. (1996). Genetic predisposition and parameters of malignant progression in K14–HPV16 transgenic mice. Am. J. Pathol. *149*, 1899–1917.

Coussens, L.M., Raymond, W.W., Bergers, G., Laig-Webster, M., Behrendtsen, O., Werb, Z., Caughey, G.H., and Hanahan, D. (1999). Inflammatory mast cells up-regulate angiogenesis during squamous epithelial carcinogenesis. Genes Dev. *13*, 1382–1397.

Coussens, L.M., Tinkle, C.L., Hanahan, D., and Werb, Z. (2000). MMP-9 supplied by bone marrow-derived cells contributes to skin carcinogenesis. Cell *103*, 481–490.

Daniel, D., Meyer-Morse, N., Bergsland, E.K., Dehne, K., Coussens, L.M., and Hanahan, D. (2003). Immune enhancement of skin carcinogenesis by CD4+ T cells. J. Exp. Med. *197*, 1017–1028.

de Visser, K.E., Korets, L.V., and Coussens, L.M. (2004). Early neoplastic progression is complement independent. Neoplasia *6*, 768–776.

Dunn, G.P., Bruce, A.T., Ikeda, H., Old, L.J., and Schreiber, R.D. (2002). Cancer immunoediting: from immunosurveillance to tumor escape. Nat. Immunol. *3*, 991–998.

Ernst, P.B., and Gold, B.D. (2000). The disease spectrum of Helicobacter pylori: the immunopathogenesis of gastroduodenal ulcer and gastric cancer. Annu. Rev. Microbiol. *54*, 615–640.

Firestein, G.S. (2003). Evolving concepts of rheumatoid arthritis. Nature *423*, 356–361.

Giraudo, E., Inoue, M., and Hanahan, D. (2004). An amino-bisphosphonate targets MMP-9-expressing macrophages and angiogenesis to impair cervical carcinogenesis. J. Clin. Invest. *114*, 623–633.

Gould, H.J., Sutton, B.J., Beavil, A.J., Beavil, R.L., McCloskey, N., Coker, H.A., Fear, D., and Smurthwaite, L. (2003). The biology of IGE and the basis of allergic disease. Annu. Rev. Immunol. *21*, 579–628.

Greten, F.R., Eckmann, L., Greten, T.F., Park, J.M., Li, Z.W., Egan, L.J., Kagnoff, M.F., and Karin, M. (2004). IKKbeta links inflammation and tumorigenesis in a mouse model of colitis-associated cancer. Cell *118*, 285–296.

Hartmann, K., Henz, B.M., Kruger-Krasagakes, S., Kohl, J., Burger, R., Guhl, S., Haase, I., Lippert, U., and Zuberbier, T. (1997). C3a and C5a stimulate chemotaxis of human mast cells. Blood *89*, 2863–2870.

Hebeis, B.J., Klenovsek, K., Rohwer, P., Ritter, U., Schneider, A., Mach, M., and Winkler, T.H. (2004). Activation of virus-specific memory B cells in the absence of T cell help. J. Exp. Med. *199*, 593–602.

Hogarth, P.M. (2002). Fc receptors are major mediators of antibody based inflammation in autoimmunity. Curr. Opin. Immunol. *14*, 798–802.

Hu, L., Dixit, V.D., de Mello-Coelho, V., and Taub, D.D. (2004). Age-associated alterations in CXCL1 chemokine expression by murine B cells. BMC Immunol. *5*, 15.

Ibanez, O.M., Mouton, D., Ribeiro, O.G., Bouthillier, Y., De Franco, M., Cabrera, W.H., Siqueira, M., and Biozzi, G. (1999). Low antibody responsiveness is found to be associated with resistance to chemical skin tumorigenesis in several lines of Biozzi mice. Cancer Lett. *136*, 153–158.

Ishibashi, T., Yamada, H., Harada, S., Harada, Y., Takamoto, M., and Sugiyama, K. (1978). Inhibition and promotion of tumor growth by BCG: evidence for stimulation of humoral enhancing factors by BCG. Int. J. Cancer *21*, 67–71.

Ji, H., Ohmura, K., Mahmood, U., Lee, D.M., Hofhuis, F.M., Boackle, S.A., Takahashi, K., Holers, V.M., Walport, M., Gerard, C., et al. (2002). Arthritis critically dependent on innate immune system players. Immunity *16*, 157–168.

Kupper, T.S., and Fuhlbrigge, R.C. (2004). Immune surveillance in the skin: mechanisms and clinical consequences. Nat. Rev. Immunol. *4*, 211–222.

Lee, D.M., Friend, D.S., Gurish, M.F., Benoist, C., Mathis, D., and Brenner, M.B. (2002). Mast cells: a cellular link between autoantibodies and inflammatory arthritis. Science *297*, 1689–1692.

Lenert, P., Brummel, R., Field, E.H., and Ashman, R.F. (2005). TLR-9 activation of marginal zone B cells in lupus mice regulates immunity through increased IL-10 production. J. Clin. Immunol. *25*, 29–40.

Liu, Z., Diaz, L.A., Troy, J.L., Taylor, A.F., Emery, D.J., Fairley, J.A., and Giudice, G.J. (1993). A passive transfer model of the organ-specific autoimmune disease, bullous pemphigoid, using antibodies generated against the hemidesmosomal antigen, BP180. J. Clin. Invest. *92*, 2480–2488.

Locksley, R.M., Reiner, S.L., Hatam, F., Littman, D.R., and Killeen, N. (1993). Helper T cells without CD4: control of leishmaniasis in CD4-deficient mice. Science *261*, 1448–1451.

Mombaerts, P., Iacomini, J., Johnson, R.S., Herrup, K., Tonegawa, S., and Papaioannou, V.E. (1992). RAG-1-deficient mice have no mature B and T lymphocytes. Cell *68*, 869–877.

Nyhus, J.K., Wolford, C.C., Friece, C.R., Nelson, M.B., Sampsel, J.W., and Barbera-Guillem, E. (2001). IgG-recognizing shed tumor-associated antigens can promote tumor invasion and metastasis. Cancer Immunol. Immunother. *50*, 361–372.

Pikarsky, E., Porat, R.M., Stein, I., Abramovitch, R., Amit, S., Kasem, S., Gutkovich-Pyest, E., Urieli-Shoval, S., Galun, E., and Ben-Neriah, Y. (2004). NF-kappaB functions as a tumour promoter in inflammation-associated cancer. Nature *431*, 461–466.

Qin, Z., and Blankenstein, T. (2004). A cancer immunosurveillance controversy. Nat. Immunol. *5*, 3–4.

Rahemtulla, A., Fung-Leung, W.P., Schilham, M.W., Kundig, T.M., Sambhara, S.R., Narendran, A., Arabian, A., Wakeham, A., Paige, C.J., Zinkernagel, R.M., et al. (1991). Normal development and function of CD8+ cells but markedly decreased helper cell activity in mice lacking CD4. Nature *353*, 180–184.

Rhee, J.S., Diaz, R., Korets, L., Hodgson, J.G., and Coussens, L.M. (2004). TIMP-1 alters susceptibility to carcinogenesis. Cancer Res. *64*, 952–961.

Sato, S., Fujimoto, M., Hasegawa, M., Takehara, K., and Tedder, T.F. (2004). Altered B lymphocyte function induces systemic autoimmunity in systemic sclerosis. Mol. Immunol. *41*, 1123–1133.

Schaumburg-Lever, G., Rule, A., Schmidt-Ullrich, R., and Lever, W.F. (1975). Ultrastructural localization of in vivo bound immunoglobulins in bullous pemphigoid—a preliminary report. J. Invest. Dermatol. *64*, 47–49.

Schilham, M.W., Fung-Leung, W.P., Rahemtulla, A., Kuendig, T., Zhang, L., Potter, J., Miller, R.G., Hengartner, H., and Mak, T.W. (1993). Alloreactive cytotoxic T cells can develop and function in mice lacking both CD4 and CD8. Eur. J. Immunol. *23*, 1299–1304.

Schreiber, H., Wu, T.H., Nachman, J., and Rowley, D.A. (2000). Immunological enhancement of primary tumor development and its prevention. Semin. Cancer Biol. *10*, 351–357.

Shacter, E., and Weitzman, S.A. (2002). Chronic inflammation and cancer. Oncology *16*, 217–226.

Siegel, C.T., Schreiber, K., Meredith, S.C., Beck-Engeser, G.B., Lancki, D.W., Lazarski, C.A., Fu, Y.X., Rowley, D.A., and Schreiber, H. (2000). Enhanced growth of primary tumors in cancer-prone mice after immunization against the mutant region of an inherited oncoprotein. J. Exp. Med. *191*, 1945–1956.

Sylvestre, D.L., and Ravetch, J.V. (1996). A dominant role for mast cell Fc receptors in the Arthus reaction. Immunity *5*, 387–390.

Takanami, I., Takeuchi, K., and Naruke, M. (2000). Mast cell density is associated with angiogenesis and poor prognosis in pulmonary adenocarcinoma. Cancer *88*, 2686–2692.

Thun, M.J., Henley, S.J., and Gansler, T. (2004). Inflammation and cancer: an epidemiological perspective. Novartis Found. Symp. *256*, 6–21.

Toth-Jakatics, R., Jimi, S., Takebayashi, S., and Kawamoto, N. (2000). Cutaneous malignant melanoma: correlation between neovascularization and peritumor accumulation of mast cells overexpressing vascular endothelial growth factor. Hum. Pathol. *31*, 955–960.

Turini, M.E., and DuBois, R.N. (2002). Cyclooxygenase-2: a therapeutic target. Annu. Rev. Med. *53*, 35–37.

van Kempen, L.C.L., Rhee, J.S., Dehne, K., Lee, J., Edwards, D.R., and Coussens, L.M. (2002). Epithelial carcinogenesis: dynamic interplay between neoplastic cells and their microenvironment. Differentiation *70*, 610–623.

Viau, M., and Zouali, M. (2005). B-lymphocytes, innate immunity, and autoimmunity. Clin. Immunol. *114*, 17–26.

Woodley, D.T., Briggaman, R.A., O'Keefe, E.J., Inman, A.O., Queen, L.L., and Gammon, W.R. (1984). Identification of the skin basement-membrane autoantigen in epidermolysis bullosa acquisita. N. Engl. J. Med. *310*, 1007–1013.